minerals

MDPI

Article

Improving High-Alumina Iron Ores Processing via the Investigation of the Influence of Alumina Concentration and Type on High-Temperature Characteristics

Yuxiao Xue [1], Jian Pan [1,*], Deqing Zhu [1], Zhengqi Guo [1], Congcong Yang [1], Liming Lu [2] and Hongyu Tian [1]

[1] School of Minerals Processing and Bioengineering, Central South University, Changsha 410083, China; yxxue@csu.edu.cn (Y.X.); dqzhu@csu.edu.cn (D.Z.); guozqcsu@csu.edu.cn (Z.G.); smartyoung@csu.edu.cn (C.Y.); hytian@csu.edu.cn (H.T.)

[2] CSIRO Mineral Resources, Pullenvale, PO Box 883, Kenmore Qld 4069, Australia; liming.lu@csiro.au

* Correspondence:pjcsu@csu.edu.cn; Tel.: +8613873142654.

Received: 19 July 2020; Accepted: 9 September 2020; Published: 11 September 2020

Abstract: Aiming at the effective utilization of the abundant high-alumina iron ores with low iron grade, the influence of alumina concentration and type on high-temperature characteristics was clarified based on the analyses of eight typical iron ores. The results indicate that high-temperature characteristics of iron ores in various alumina types are different. Higher Al_2O_3 concentration is deleterious to assimilability and liquid phase fluidity, but the influence extent of each alumina type is substantially different. Kaolinite ($Al_2O_3{\cdot}2SiO_2{\cdot}2H_2O$) contributes to correspondingly better assimilability, followed by hercynite ($Fe(Fe, Al)_2O_4$), gibbsite ($Al(OH)_3$), diaspore ($AlO(OH)$), and free state alumina (Al_2O_3) in turn. Diaspore promotes relatively higher liquid phase fluidity, followed by kaolinite, free state alumina, and hercynite, while gibbsite possesses the maximum adverse impact. Kaolinite and hercynite are more beneficial to form dendritic or acicular silico-ferrite of calcium and alumina (SFCA) with high strength due to the better reactivity, and gibbsite and diaspore lead to more formation of relatively lower strength lamellar or tabular SFCA, while free state alumina is preferable to form disseminated SCFA with rather poorer strength. Kaolinite and hercynite are the most desirable alumina types for sintering rather than free state alumina.

Keywords: high-alumina iron ores; alumina concentration; alumina type; high-temperature characteristics; reactivity; effective utilization

1. Introduction

Due to the huge steel production and high iron ores mining cost in China, over 80% of the iron ores are imported from Australia, Brazil, South Africa, and India to meet the growing needs of steel production in China according to the data of National Bureau of Statistics. However, with the depletion of high-grade iron ore resources, alumina concentration of the imported iron ores, particularly for Indian iron ores, is increasing gradually leading to the increment in Al_2O_3 content of iron ore sinter, which constitutes a major proportion of blast furnace burden [1–3]. This would lead to the deterioration of gas permeability in blast furnace, the decrease of slag fluidity and reducibility of sinter and the increase of coke consumption and sulphur load [4–6]. It is not only deleterious to the blast furnace smelting process but also has a negative impact on steel quality in the subsequent

steelmaking process. Hence, it is essential to effectively utilize the abundant high-alumina iron ores with low iron grade.

As confirmed in the literatures [7–12], the increase of Al_2O_3 content is expected to be detrimental to the sintering performance of iron ores due to the low reactivity of alumina bearing minerals and high viscosity of primary melts. Therefore, it is necessary to investigate the action mechanism of alumina on iron ore sintering. As is well known, high-temperature characteristics of iron ores are identified as the basic indexes to evaluate the impact of iron ore properties on the sintering process as well as the output and quality of sinter through the interaction and consolidation between iron ores and fluxes, which mainly include assimilability, liquid phase fluidity, and characteristics of the bonding matrix [13–17]. The assimilability is identified as the ability of iron ore powders reacting with CaO during sintering, indicating the difficulty of liquid phase formation in the sintering process [18,19]. Liquid phase fluidity represents the effective bonding behavior of liquid phase [20,21]. Characteristics of the bonding matrix act as the generative properties of the bonding matrix mainly including its morphology, component, and formation amount [22–24]. The product sinter with high strength and good reducibility is desired for blast furnace production. The iron ore sintering process is mainly subject to the bonding phases which can effectively bond with solid phases such as hematite and magnetite to form the product sinter with good strength. In addition, it is well known that sinter strength is determined by the self-strength of the bonding phases and consolidation behavior of solid phases by liquid phases [25]. In addition, silico-ferrite of calcium and alumina (SFCA) is regarded as the most desirable bonding phase formed from a partly liquid state due to its high self-strength and good reducibility [26]. Thus, the formation ability and fluidity of liquid phase and characteristics of the bonding matrix are the key factors on iron ore sintering. Great importance should be given to the influence of alumina on high-temperature characteristics of iron ores.

Many researches on high-temperature characteristics of iron ores with various alumina concentration have been carried out [18–29]. It is found that high Al_2O_3 content tends to promote the lowest assimilation temperature and namely weakens the assimilability [18,19]. Increased alumina concentration increases the viscosity and decreases the fluidity of liquid phase [20,21,27,28]. According to the previous studies [22–24,29], the increasing Al_2O_3 content contributes to the formation of SFCA, leading to a higher proportion of SFCA in sinter. However, the excessive increase of Al_2O_3 content (>1.0%) is expected to result in a drastic deterioration in the properties of SFCA. Namely, the amount of sheet-like, columnar, and blocky SFCA with lower mechanical strength is increased significantly, while a substantial reduction in the amount of dendritic and eutectic SFCA with higher strength is detected [30–33]. Taking into account the impact of alumina concentration on high-temperature characteristics and the different alumina types in iron ores, considerable emphasis has therefore been placed on the influence of alumina types on high-temperature characteristics recently. As indicated in the reference [34], Sierra Leone ore, a high alumina iron ore containing alumina in the form of alumogoethite and gibbsite, possessed poor assimilability and liquid phase fluidity. This was further supported by the investigations [35,36]. On this basis, it was proved that gibbsite ($Al(OH)_3$) was more conducive to assimilability than kaolinite ($Al_2O_3{\cdot}2SiO_2{\cdot}2H_2O$) [37]. In addition, gibbsite gangues yielded low-Al_2O_3-SFCA with high liquid phase fluidity, while kaolinite gangues produced high-Al_2O_3-SFCA with low liquid phase fluidity. Furthermore, the relative effect of gibbsite, kaolinite, and aluminous goethite ($[Al_xFe_{(1-x)}]OOH$) as alumina sources on formation mechanisms of SFCA was studied [38]. It was demonstrated that kaolinite was favorable to maximize the formation of higher strength SFCA followed by aluminous goethite and gibbsite in turn, attributed to the different reactivity of various types of alumina.

However, there are still many problems to be settled. On the one hand, although some researchers are paying attention to the influence of alumina type recently, they always expound the action mechanism of different alumina types by adopting some kinds of alumina-rich iron ores. This would lead to ambiguous results due to that the used iron ores generally possess several types of alumina such as kaolinite, gibbsite, and hercynite. Hence, as researchers aim at the influence of one

type of alumina, other types of alumina could cause interference and it would be hard to accurately clarify the influence of specific alumina type. On the other hand, many investigations are mainly about the alumina types of kaolinite, hercynite, or gibbsite while other alumina types such as free state alumina and diaspore are rarely involved. The influence of alumina concentration and type on assimilability, liquid phase fluidity, and characteristics of the bonding matrix has not been simultaneously investigated. The previous studies generally focus on the influence of alumina concentration and type on one or two high-temperature characteristics. Comprehensive investigations have not been conducted to clearly elucidate the influence of all alumina types on high-temperature characteristics of iron ores. In order to solve the problems above, a new research methodology has been proposed in this paper to investigate the influence of alumina concentration and type on the high-temperature characteristics of iron ores by five Al-additives substituting for various types of alumina including free state alumina, gibbsite, kaolinite, hercynite, and diaspore, respectively. Each Al-additive only contains one type of alumina, which contributes to clearly distinguish the influence of different types of alumina. Thus, we can identify the alumina types which are more beneficial for iron ore sintering. This would also be favorable to select the appropriate alumina-rich iron ores for sinter production.

In this paper, based on the analyses of eight imported iron ores widely used in the steel industry of China, the differences of high-temperature characteristics of the eight iron ores including assimilability, liquid phase fluidity, and characteristics of the bonding matrix were ascertained, and the influence of five aluminum types, i.e., free state alumina, gibbsite, kaolinite, hercynite, and diaspore, on high-temperature characteristics was investigated comprehensively via analogue sintering tests conducted in the horizontal tube furnace to provide good guidance for the rational utilization of the abundant high-alumina iron ores.

2. Materials and Methodology

2.1. Characterization Techniques

Characterization techniques mainly include the determination methods of chemical compositions and mineralogy. The chemical compositions were analyzed by X-ray fluorescence (XRF, Axios mAX XRF Spectrometer, PANalytical B.V., Alemlo, Holland). Mineralogical analyses consist of the mineral phase identification and microstructure analysis. The former was clarified by X-ray diffraction (XRD, Simens D500 automatic X-ray diffractometer, Siemens AG, Berlin, Germany) with a copper target, which was operated at 40 kV and 250 mA in step mode with 0.02° 2θ step and a count time of 0.5 s per step over a 2θ range from 10 to 80°. The XRD data were analyzed by the software of MDI Jade 6.5 via the quantification approach of Rietveld refinement. The latter was revealed by the means of the optical microscope and scanning electron microscopy after the preparation of samples. Firstly, sintered tablets were embedded by the acrylic powder and epoxy resin curing agent with the ratio of 1:1.8 in the relevant rubber mold and then made into cylindrical samples with 30 mm in diameter and 15 mm in height at room temperature. After polished by the semi-automatic grinding and polishing machine (Tegramin-25, Struers Ltd., Shanghai, Denmark), the samples were placed in the optical microscope (Leica DM4500P, Leica Camera AG, Solms, Germany) by using reflected plane polarized light for optical photographs. The mineral compositions and porosity of sintered tablets were determined by the software of Image-Pro Plus 6.0 via the area calculation method. Then, scanning electron microscopy and energy dispersive spectrum (SEM-EDS) analyses were finished by the aid of environmental scanning electron microscope (ESEM, FEI Quanta-200, FEI, Hillsboro,OR, USA) equipped with an EDAX energy dispersive X-ray spectroscopy (EDS) detector. The detailed parameters were shown as follows: Type of imagery: Back scattered electron mode; beam current: Energy spectrum spot or line scan (500 nA); accelerating voltage: 20 kv; counting times: 50 s. The spectra were quantified to give chemical analyses by using the standardless quantification mode. The distributions of Al_2O_3 (chemical component) over mineralogical phases were determined

quantitatively by the means of FEI scanning electron microscope (FEI, Hillsboro, OR, USA) equipped with a mineral liberation analyzer (MLA).

2.2. Raw Materials

2.2.1. Iron Ores

Table 1 presents the chemical compositions of the iron ore samples. Eight imported iron ores are adopted including three Australian ores (A, B, and C), two Brazilian ores (D and E), two African ores (F and G), and one Indian ore (H). It is found that Al_2O_3 contents of eight iron ores are all not less than 1.00%, even which in iron ore F comes up to as high as 5.95%. Meanwhile, iron ores A, C, and F possess a lower iron grade and higher loss on ignition (LOI), contributing to the formation of porous sinter and then weakening the sinter strength [36]. In addition, SiO_2 contents of iron ores are quite different and the influence on high-temperature characteristics of iron ores needs to be taken into account [30,39]. The low contents of MgO, P, and S of iron ores are beneficial to the sintering process [7]. Moreover, eight iron ores are all crushed to −0.5 mm for avoiding the interference of size distributions on experiments. The detailed data of size distributions and mineralogy of iron ores are shown in Table A1, Figures A1 and A2. The alumina distributions in iron ores are presented in Table 2.

Table 1. Chemical compositions of iron ores (wt%).

Source Regions	Iron Ores	TFe	FeO	SiO_2	CaO	Al_2O_3	MgO	P	S	LOI *
Australia	A	56.21	0.36	6.43	0.09	2.55	0.06	0.061	0.010	9.73
	B	61.11	0.54	3.61	0.08	2.27	0.11	0.072	0.022	6.11
	C	58.09	0.30	5.27	0.10	1.59	0.05	0.054	0.014	9.76
Brazil	D	61.71	0.80	6.64	0.14	1.66	0.06	0.061	0.010	2.81
	E	65.42	0.25	2.05	0.06	1.00	0.11	0.046	0.010	1.74
Africa	F	57.26	0.36	2.04	0.04	5.95	0.03	0.076	0.056	9.18
	G	63.45	0.27	6.18	0.05	1.74	0.03	0.048	0.016	1.07
India	H	62.67	0.27	3.35	0.03	3.03	0.03	0.049	0.010	3.59

* LOI: Loss on ignition.

Table 2. Alumina distributions in iron ores (wt%).

Alumina Distribution	Hematite	Goethite	Gibbsite	Kaolinite
A	10.2	89.8	-	-
B	3.08	60.36	17.62	18.94
C	7.55	55.97	-	36.48
D	0	25.3	74.7	-
E	0	25.85	45.85	28.3
F	0	40.67	59.33	-
G	0	11.49	-	88.51
H	16.83	13.53	43.89	25.75

2.2.2. Al-Additives

Table 3 demonstrates the chemical compositions of the adopted Al-additives including Al_2O_3 and $Al(OH)_3$ pure reagents, washed kaolinite, synthetic hercynite, and diasporic bauxite. The former two Al-additives possess a chemical grade, both produced from the Aladdin company. The latter three Al-additives are supplied by Chinese steel enterprises. The Al_2O_3 reagent with Al_2O_3 content of 94.42% is used to represent free state alumina. The $Al(OH)_3$ reagent contains 64.07% Al_2O_3, which is adopted to substitute for gibbsite, and its high LOI of 33.84% is adverse to the sintering process [36].

Washed kaolinite assaying 44.80% SiO_2, 36.20% Al_2O_3, and 15.76% LOI is obtained by the water washing process and its high SiO_2 content is expected to be favorable to the formation of liquid phases with a low melting point [18,22]. Synthetic hercynite mainly consisting of 48.38% Al_2O_3 and 34.35% total iron is formed through the electric melting process and the higher iron grade would contribute to rising the amount of SFCA [40,41]. Diasporic bauxite mainly possesses 70.27% Al_2O_3, 10.08% SiO_2, and 14.34% LOI. As evidenced in Figure 1, washed kaolinite, synthetic hercynite, and diasporic bauxite can be exactly used as the substitutions for various types of alumina, i.e., kaolinite, hercynite, and diaspore, respectively. Moreover, the contents of particles passing 0.074 mm of five Al-additives are maintained at 100% for analogue sintering tests. The detailed data of size distributions are shown in Table A2.

Table 3. Chemical compositions of Al-additives (wt%).

Al-Additives	TFe	FeO	SiO_2	CaO	Al_2O_3	MgO	P	TiO_2	LOI *
Al_2O_3 reagent	0.01	-	-	-	94.42	-	-	-	5.00
$Al(OH)_3$ reagent	-	-	-	-	64.07	-	-	-	33.84
Washed kaolinite	1.02	-	44.80	0.01	36.20	0.03	0.022	0.20	15.76
Synthetic hercynite	34.25	20.94	0.96	0.12	48.38	0.99	0.170	0.65	−3.32
Diasporic bauxite	1.23	-	10.08	0.40	70.27	-	-	2.26	14.34

* LOI: Loss on ignition.

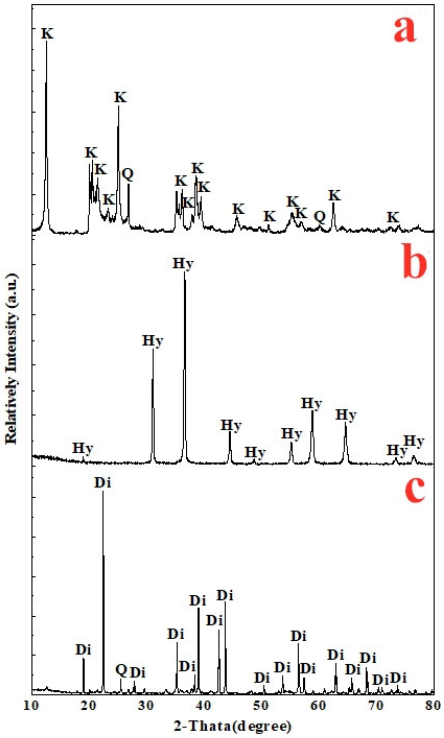

Figure 1. X-ray diffraction patterns of washed kaolinite (**a**), synthetic hercynite (**b**), and diasporic bauxite (**c**) (K: Kaolinite; Q: Quartz; Hy: Hercynite; Di: Diaspore).

2.3. Experimental Procedure

The diagram of the main experimental setup (horizontal tube furnace) is demonstrated in Figure 2. In the experiments, the horizontal tube furnace (GSL-1400X, Kejing Material Technology Co., Ltd, Hefei, China) is adopted produced by a Chinese manufacturer with the heating rate of 10 °C/min. It

contains tow temperature zones, i.e., preheating and roasting zones. They are heated by SiC and MoSi nanorods, respectively. The furnace tube is a high-purity corundum tube with 60 mm in diameter and 1000 mm in length.

In addition, due to the relatively lower Al_2O_3 content of 1.0%, iron ore E is adopted as the base iron ore to investigate the influence of alumina concentration and type on high-temperature characteristics by adding different Al-additives. The pure reagents of CaO and $Ca(OH)_2$ with 100% passing −0.074 mm are adopted as fluxes to adjust the basicity of the sinter mixture. As Al-additives are added, the SiO_2 pure reagent with the same size distribution is used to maintain SiO_2 content of the sinter mixture at 5.0%. The experimental run table with a clear inventory of the starting material compositions for all the experiments is placed in Tables A3 and A4. The detail methods are shown as follows.

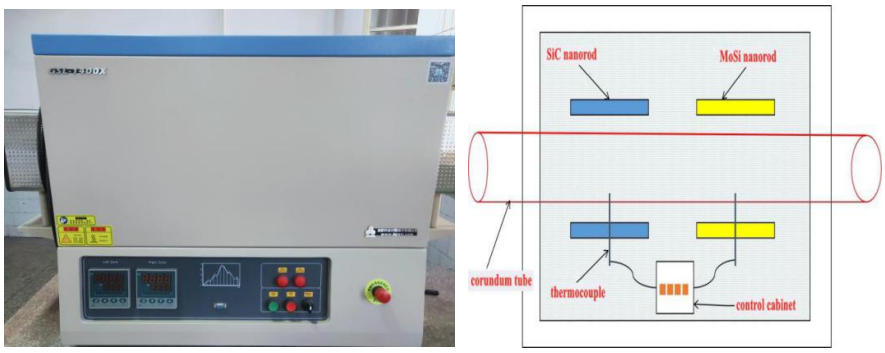

Figure 2. The diagram of the main experimental setup (horizontal tube furnace).

2.3.1. Assimilability

In order to evaluate the assimilability of the eight iron ores, the iron ore sample and CaO pure reagent were separately mixed and compressed into the tablets with 8 and 25 mm in diameter, respectively and both 10 mm in height at a set pressure of 200 N. The dried iron ore tablet was put up on the CaO tablet and then put into the horizontal tube furnace and roasted at various temperatures (1250–1390 °C) for 5 min in the air atmosphere. Then, the tablets were slowly removed from the furnace in 5 min and then cooled to room temperature in the air. The lowest assimilation temperature acting as the valuation index for the assimilability was obtained, where the obvious corrosion firstly appeared on the contact interface between iron ore and CaO tablets. The lower the lowest assimilation temperature was, the better the assimilability was [42].

To clarify the influence of alumina concentration and type on the assimilability, five Al-additives were blended with the iron ore E sample to maintain Al_2O_3 content at 1.5%, 2.0%, 2.5%, 3.0%, and 3.5%, respectively. In the meantime, the SiO_2 pure reagent was added to retain the SiO_2 content of the sinter mixture at 5.0%. The followed test processes were the same as the above.

2.3.2. Liquid Phase Fluidity

In order to determine the liquid phase fluidity of the eight iron ores, the iron ore sample and $Ca(OH)_2$ pure reagent were mixed with water at 4.0 basicity and compressed into tablets with 10 mm in diameter and 8 mm in height at a set pressure of 200 N. After dried, the ore tablet was placed up on the corundum tablet with 40 mm in diameter and 2 mm in height and then put into the horizontal tube furnace, roasted at 1310 °C for 5 min in the air atmosphere. After cooled to room temperature via the same cooling method, the liquid phase fluidity index was measured according to the literature [27]. The higher fluidity index contributed to the better liquid phase fluidity.

To proclaim the influence of alumina concentration and type on the liquid phase fluidity, Al-additives, iron ore E, $Ca(OH)_2$, and SiO_2 pure reagents were blended together according to the fixed

proportions to obtain the sinter mixture. The Al_2O_3 content of the mixture was maintained at 1.5%, 2.0%, 2.5%, 3.0%, and 3.5%, respectively by adjusting the proportion of Al-additives, whereas the SiO_2 content and the basicity of the mixture were remained at 5.0% and 4.0%, respectively. The following test processes were same as the above.

2.3.3. Characteristics of the Bonding Matrix

In order to investigate the characteristics of the bonding matrix of the eight iron ores, the iron ore sample and $Ca(OH)_2$ pure reagent were mixed with water at 3.0 basicity and compressed into tablets with 10 mm in diameter and 8 mm in height under the 200 N pressure. Then, eight dried tablets were put into the porcelain boat with a volume of 8 mL and roasted at 1310 °C for 5 min in the air atmosphere in the horizontal tube furnace. After cooled to room temperature via the same cooling method, the mineralogy of the sintered tablets was determined to reveal the characteristics of the bonding matrix of eight iron ores by means of the methods in Section 2.1.

As shown in Figure 3, interface reaction tests were carried out to clarify the influence of alumina concentration and type on the characteristics of the bonding matrix at nature basicity. The iron ore E sample and five Al-additives were compressed into tablets with 10 mm in diameter and 8 mm in height at a set pressure of 200 N, respectively. After dried, the iron ore tablet was put upon the Al-additive tablet and roasted at 1310 °C in the air atmosphere for 5 min in the horizontal tube furnace. After cooled to room temperature via the same cooling method, the mineralogy of reaction interface of the tablets was investigated in accordance with the methods in Section 2.1.

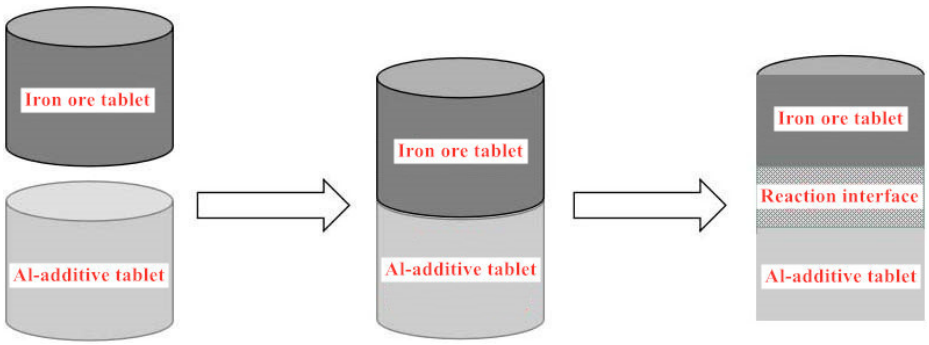

Figure 3. Schematic diagram of interface reaction test.

3. Results and Discussion

3.1. High-Temperature Characteristics of Iron Ores in Different Types

In this part, high-temperature characteristics of the eight iron ores were carried out, providing guidance for the follow-up investigations of the influence of alumina concentration and type on the high-temperature characteristics.

3.1.1. Assimilability of Iron Ores

Figure 4 compares the assimilability of eight iron ores. As corroborated in the reference [18], the assimilability of iron ores is dominated by iron ore types and its chemistry. High LOI contributes to the formation of porous structure, which can improve kinetic conditions of the reaction between Fe_2O_3 and CaO and then promote the assimilability of iron ores. The excessive Al_2O_3 content is harmful to the assimilability of iron ores, attributed to the elevation of melting point of liquid phases. Overall, Australian iron ores possess better assimilability, followed by Indian and Brazilian iron ores, while the assimilability of African iron ores is rather poorer, agreeing with the results of the previous investigation [34].

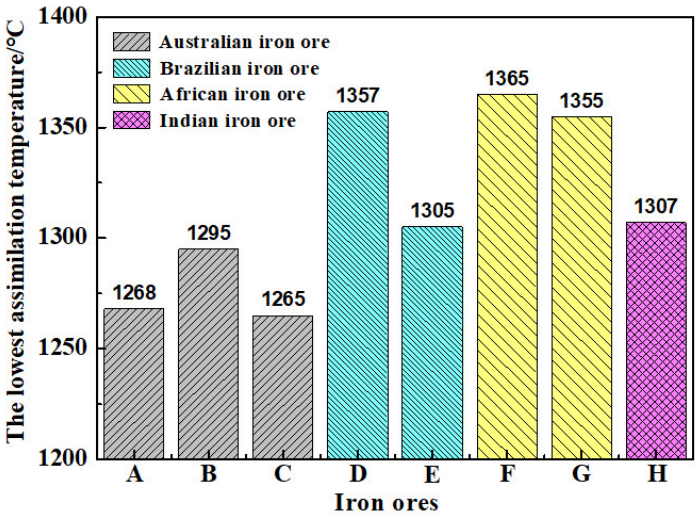

Figure 4. Assimilability of iron ores in various alumina types.

On the other hand, alumina types of iron ores also affect the assimilability as shown in Figure 4. Iron ore A possesses higher Al_2O_3 content and lower LOI compared with iron ore C. However, the lowest assimilation temperature of iron ore A is higher than that of iron ore C. As investigated in Figure A2 and Table 2, the alumina of iron ore A is in the form of hercynite while alumina types in iron ore C include hercynite and kaolinite. Thus, kaolinite is expected to lead to better assimilability than hercynite. Similarly, compared to the assimilability of iron ore D with that of G, it is supposed that kaolinite contributes to better assimilability than gibbsite. However, the effect of alumina types on assimilability could not be expounded clearly due to that multiple types of aluminum exist in iron ores. Hence, it is of great necessity to quantitatively reveal the effect of each alumina type on the assimilability of iron ores.

3.1.2. Liquid Phase Fluidity of Iron Ores

Figures 5 and 6 illustrate the liquid phase fluidity of iron ores in various alumina types. Brazilian iron ore D and African iron ore G possess better liquid phase fluidity with fluidity indexes of 7.76 and 7.67, respectively, followed by Australian iron ores C, A, and B with fluidity indexes of 6.29, 5.91, and 1.26, respectively. The liquid phase fluidity of Brazilian iron ore E, African iron ore F, and Indian iron ore H is rather poorer. As indicated in the previous studies [40,43], SiO_2 is beneficial to the liquid phase fluidity due to its favorable impact on the flowing of liquid phase, while Al_2O_3 presents the opposite rule attributed to the increase of liquid phase viscosity. Combined with the relevant results in Section 4 of Figure A3, it is also found that SiO_2 and Al_2O_3 both have great impact on liquid phase fluidity. Thus, the liquid phase fluidity of iron ores D and G with higher SiO_2 content and low Al_2O_3 content is superior to that of the rest iron ores.

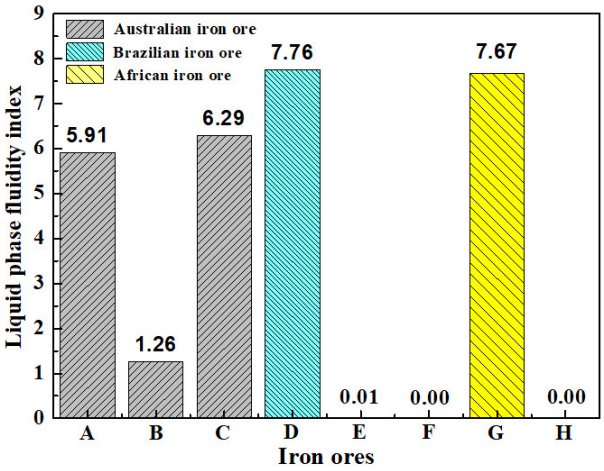

Figure 5. Liquid phase fluidity index of iron ores in various alumina types.

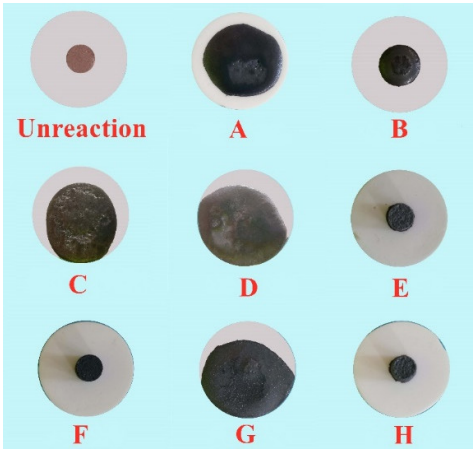

Figure 6. Schematic diagram of liquid phase fluidity of iron ores in various alumina types.

However, some anomalies of liquid phase fluidity could not be explained by the above viewpoint. For example, iron ores B and H contain similar SiO_2 and Al_2O_3 contents while the liquid phase fluidity of the two ores is different. This is probably due to the difference of alumina types. As confirmed in Section 2 of Figure A2 and Table 2, alumina types of iron ores B and H both include hercynite, gibbsite, and kaolinite, but alumina in the former is mainly in the form of hercynite with a content of 63.44% whereas most alumina of the latter is enriched in gibbsite. Thus, it is expected that hercynite is more favorable to maintain better liquid phase fluidity compared with gibbsite, which will be validated in the follow-up experiments.

3.1.3. Resultant Mineralogy and Microstructure of Sintered Tablets

Figure 7 presents the resultant mineralogy and microstructure of sintered tablets. Large irregular pores with thinner wall mainly exist in the sintered tablet of iron ore F and the porosity reaches as high as 66.23% due to the higher Al_2O_3 content and LOI of 5.95% and 9.18%, respectively (Table 4). Iron ores A, B, C, and H possess similar porosity of sintered tablets, but the microstructure is very different. In the sintered tablet of iron ore C, the pores primarily exhibit a large and round texture with a thin wall attributed to the relatively lower Al_2O_3 content of 1.59% while the pores in the sintered tablets of iron ores A and B tend to be elliptical with a large size. In addition, the comparatively higher Al_2O_3 content of 3.03% in iron ore H leads to the pores of its sintered tablet

converting into irregular macropores through coalescence. In addition, the porosity of the post-experimental samples of iron ores D, E, and G is lower than 30% and the microstructure of the sintered tablets is dominated by small thin-wall pores or large thick-wall pores on the account of the correspondingly lower Al_2O_3 content and LOI. It is found that the microstructure of the sintered tablets of iron ores is subject to their Al_2O_3 content and LOI, agreeing with the results of the literature [25]. Higher LOI contributes to the formation of relatively regular pores with a large size and thin wall, while irregularly interconnected pores are mostly observed in porous sintered tablets of higher Al_2O_3 content which is more unfavorable to the strength of sintered tablets.

On the other hand, the chemistry of iron ores also has a significant impact on the characteristics of the bonding matrix [1]. The sintered tablets of iron ores A, C, D, and G possess high SFCA amount of over 70% due to their higher SiO_2 content and the SFCA amount rises with the increase of Al_2O_3 content (Table 4). The similar SiO_2 and Al_2O_3 contents of the sintered tablets of iron ores B and H lead to a similar SFCA amount of about 60%. Moreover, compared to the formation amount of SFCA of the sintered tablet of iron ore E with that of iron ore F, it is found that the exorbitant Al_2O_3 content is adverse to SFCA formation on the condition of low SiO_2 content, in accordance with the results of previous investigations [9,44]. Meanwhile, the Al_2O_3 content also affects the morphology of SFCA. As shown in Figure 7, higher Al_2O_3 content promotes the emerge of coarse tabular or lamellar SFCA in the sintered tablets of iron ores F and H, while a low Al_2O_3 content is instrumental in the formation of acicular or dendritic SFCA which is identified as having higher strength [31]. Furthermore, a trace of silicate is also observed in sintered tablets with an excessive SiO_2 content.

It is much more noteworthy that the type of alumina also plays an important role in the characteristics of the bonding matrix. Comparing iron ore B with iron ore H, their Al_2O_3 and SiO_2 contents are close, however, the SFCA morphology in their sintered tablets is distinctly different, which is probably relevant to the difference of alumina type. The sintered tablet of iron ore B with alumina rich in hercynite primarily possesses acicular or dendritic SFCA, while that of iron ore H with alumina mainly in the form of gibbsite yields tabular or lamellar SFCA. It is expected that hercynite is more advantageous to form acicular or dendritic SCFA with higher strength compared with gibbsite. Likewise, the formation amount of acicular or dendritic SFCA in the sintered tablet of iron ore G is obviously higher than that of iron ore D, indicating that kaolinite has a more positive impact on the formation of higher strength SFCA than gibbsite combined with the investigations of Section 2 of Figure A2. In addition, this would then lead to different sinter strengths of iron ores. Therefore, it is significant to clarify the different influences of various alumina types on the characteristics of the bonding matrix.

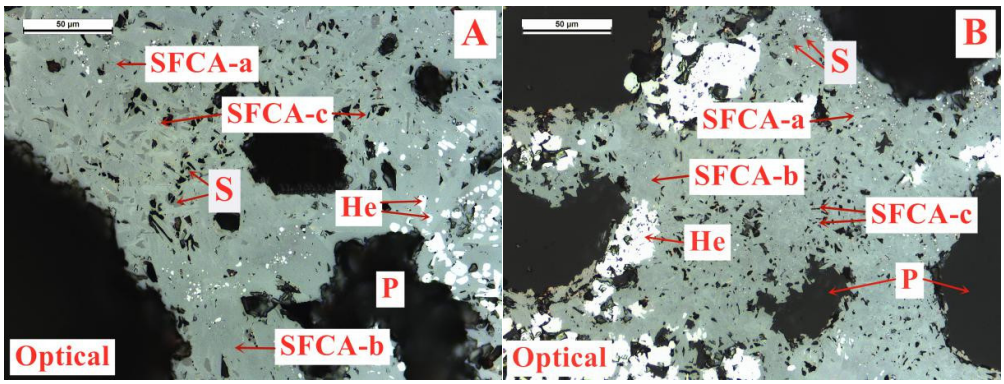

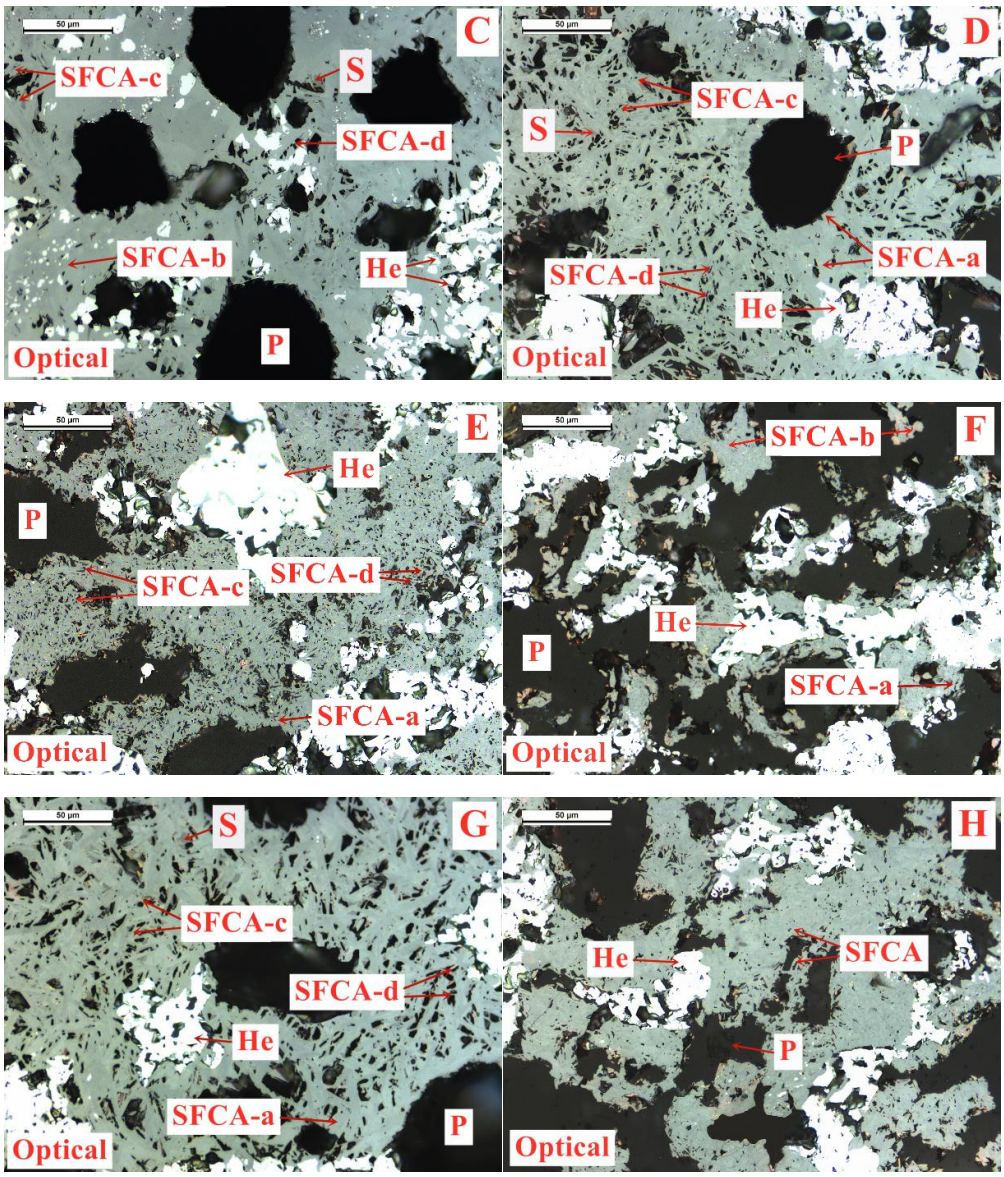

Figure 7. Characteristics of the bonding matrix in sinter tablets of various types of iron ores ((**A–H**) represent the optical photographs of iron ores A-H respectively; He: Hematite; S: Silicate; SFCA-a-Tabular: SFCA; SFCA-b-Lamellar: SFCA; SFCA-c-Dendritic: SFCA; SFCA-d-Acicular: SFCA; P: Pores).

Table 4. The mineral compositions and porosity of iron ores sinter (area: %).

Iron Ores	Porosity	Mineral Compositions		
		SFCA	Hematite	Silicate
A	50.31	92.65	4.79	2.56
B	49.97	63.54	34.74	1.72
C	45.61	70.24	25.87	3.89
D	28.96	70.26	25.65	4.09
E	21.78	46.51	53.49	-
F	66.23	26.12	73.88	-
G	28.67	72.83	21.94	5.23
H	48.07	60.88	39.12	-

Overall, although high-temperature characteristics of iron ores is certainly affected by their chemical compositions including LOI, Al_2O_3, and SiO_2 contents, it also indicates that various alumina types have different impacts on high-temperature characteristics. Kaolinite is expected to contribute to better assimilability than gibbsite and hercynite. In addition, hercynite probably leads to higher liquid phase fluidity compared with gibbsite. Meanwhile, hercynite and kaolinite are possibly more available to form acicular or dendritic SFCA with higher strength than gibbsite. Thus, it is ought to clearly reveal and verify the influence extent of each aluminum type on high-temperature characteristics.

3.2. Influence of Alumina Concentration and Type on High-Temperature Characteristics

In this section, high-temperature characteristics such as assimilability, liquid phase fluidity, and characteristics of the bonding matrix were investigated in various alumina concentrations and types by adjusting the proportions of the relevant Al-additives.

3.2.1. Influence of Alumina Concentration and Type on Assimilability

Figure 8 proclaims the influence of alumina concentration and type on assimilability. It can be seen that the lowest assimilation temperature is increased with the Al_2O_3 content corresponding to the results of the previous study [18], indicating the gradual deterioration of assimilability. However, the effect extent of each type of alumina on assimilability is quite different. At the same alumina concentration, the free state alumina possesses a more deleterious effect on assimilability, followed by diaspore, gibbsite, hercynite, and kaolinite in turn. This is also consistent with the investigations of Figure 4. Thus, for all five types of alumina with an equal Al_2O_3 content, it is confirmed that alumina in the form of kaolinite contributes to the best assimilability, while free state alumina plays the opposite role. In addition, the formation of primary liquid phase would then be suffering different influences in various alumina types, further leading to different sintering performances of iron ores.

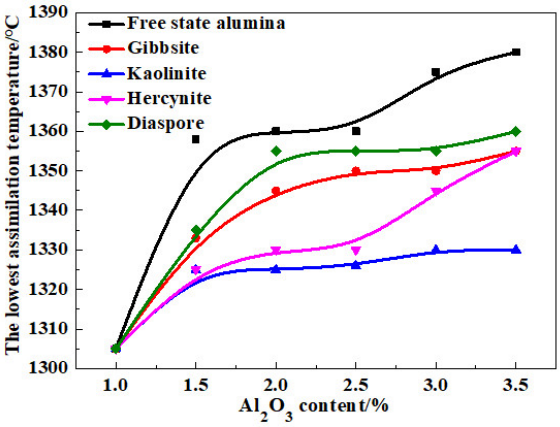

Figure 8. Influence of alumina concentration and type on assimilability.

3.2.2. Influence of Alumina Concentration and Type on Liquid Phase Fluidity

Figure 9 summarizes the impact of alumina concentration and type on liquid phase fluidity. As for alumina in the form of diaspore, kaolinite, and free state alumina, the liquid phase fluidity indexes are slightly elevated from 6.75%, 6.11%, and 5.91% to 8.43%, 7.15%, and 6.16%, respectively with the Al_2O_3 content varying from 1.5% to 2.0%, indicating the improvement of liquid phase fluidity. As the Al_2O_3 content further reaches to 3.5%, the liquid phase fluidity is substantially deteriorated, especially for kaolinite. Moreover, increasing the concentration of alumina that exists in hercynite and gibbsite gradually lowers the liquid phase fluidity.

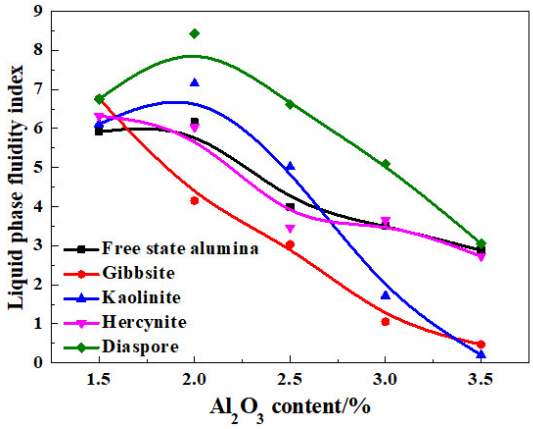

Figure 9. Influence of alumina concentration and type on liquid phase fluidity.

It is found that alumina in various types possesses different impacts on liquid phase fluidity. At a relatively lower Al_2O_3 content (<2.0%), increasing the Al_2O_3 content is favorable to liquid phase fluidity as to diaspore, kaolinite, and free state alumina. This is probably owing to that the proper addition of alumina contributes to the formation of SFCA and then weakening the adverse effect of alumina on liquid phase fluidity to some extent [22–24,29]. As the Al_2O_3 content is above 2.0%, its increase is detrimental to liquid phase fluidity for all alumina types, but the influence degrees are different. Diaspore leads to a relatively better liquid phase fluidity compared with other types of alumina while gibbsite presents the opposite rule. In addition, the negative effect extents of hercynite and free state alumina on liquid phase fluidity are very close, slightly lower than that of gibbsite. Furthermore, kaolinite promotes higher liquid phase fluidity than hercynite at the Al_2O_3 content of 1.50–2.70%. As the Al_2O_3 content is further increased, the liquid phase fluidity tends to be deteriorated

to only close to that of gibbsite, due to that its high SiO_2 content leads to the massive formation of silicate phases with high melting point such as $2CaO{\cdot}SiO_2$ and $3CaO{\cdot}SiO_2$ at exorbitant basicity (4.0) [45–47]. It should be noted that the suitable basicity is expected to be different for various alumina types. In addition, the different impacts of alumina type on liquid phase fluidity could result in different characteristics of the bonding matrix as well as the sintering performance of iron ores.

3.2.3. Influence of Alumina Concentration and Type on the Characteristics of the Bonding Matrix

Figures 10–14 reveal the influence of alumina concentration and type on characteristics of the bonding matrix by the mineralogy of reaction interface. In addition, the reactivity of each type of alumina is characterized by the interfacial width (Table 10). The greater the average width is, the better the reactivity is. In Figures 10–14, the SEM photograph (b) is obtained by the optical photograph (a) rotated 90° to the right. In the optical photograph (a), the double arrow area represents the reaction interface and its upper and lower parts are the horizons of the iron ore and Al-additive, respectively.

As shown in Figure 10 and Table 5, liquid phases are mainly composed of three types of SFCA, i.e., dendritic, lamellar, and disseminated SCFA in the reaction interface between the iron ore and free state alumina. The amount of dendritic SCFA containing as high as 55.82% Fe is rare, while the disseminated SCFA with lower iron and higher alumina contents of 46.21% and 4.05%, respectively is massively formed and mainly concentrated on the side of free state alumina tablet. Likewise, a small amount of lamellar SFCA assaying 48.13% Fe and 2.68% Al is also observed. As investigated in the previous literature [38], all of which is expected to be relevant to the poor reactivity of free state alumina with the average interfacial width of only 1.31 mm is shown in Table 10. Thus, free state alumina contributes to the abundant formation of lower strength SFCA such as disseminated SCFA.

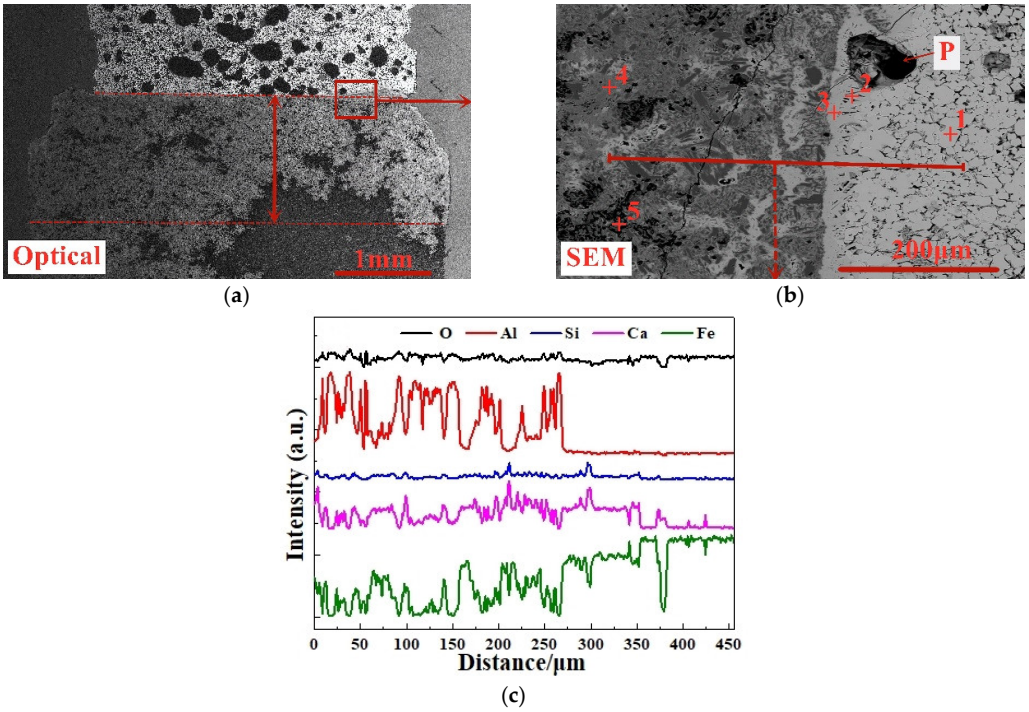

Figure 10. Effect of free state alumina on the characteristics of the bonding matrix (P: Pore; a→b: Rotate 90° to the right; (**a**,**b**) are the optical and SEM photographs of the reaction interface respectively; (**c**) is the of the photograph of line scan in (**b**)).

Table 5. EDS analysis results for areas in Figure 10b.

Area No.	Elemental Compositions/(wt%)					Mineral Phases
	Fe	Al	Si	Ca	O	
1	68.78	0.79	0.00	0.00	30.43	Hematite
2	55.82	1.67	1.23	7.33	33.95	Dendritic SFCA
3	48.13	2.68	3.02	10.79	35.38	Lamellar SFCA
4	46.21	4.05	3.27	12.88	33.59	Disseminated SFCA
5	0.00	53.33	0.00	0.00	46.67	Residual alumina

Combined with Figure 11 and Table 6, it is found that in the reaction interface between the iron ore and gibbsite, the iron contents of dendritic, lamellar, and disseminated SCFA are all increased to some degree compared with that in the reaction interface between the iron ore and free state alumina. In addition, dendritic SFCA possesses an increased formation amount, while the disseminated SCFA presents the opposite way. On the other hand, the porosity is significantly increased due to the LOI of gibbsite accounting for as high as 33.84%. Hence, although the reactivity of gibbsite with the average interfacial width of 1.61 mm (Table 10) is better than that of free state alumina, the improvement of sinter strength is likely to be much less dramatic.

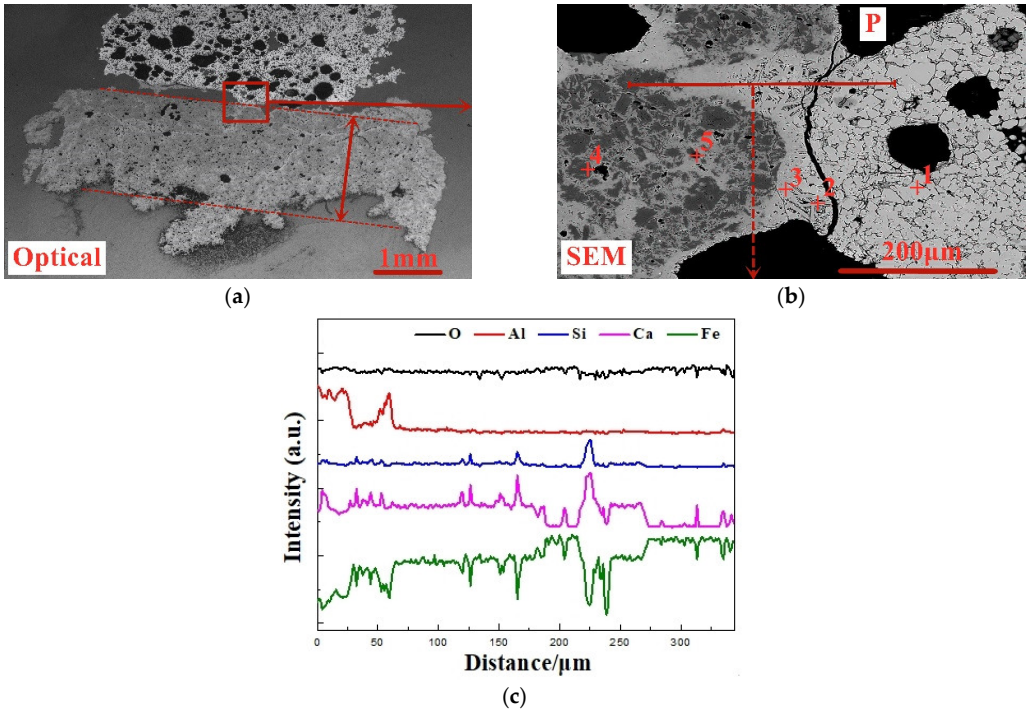

Figure 11. Effect of gibbsite on the characteristics of the bonding matrix (P: Pore; a→b: Rotate 90° to the right; (**a**,**b**) are the optical and SEM photographs of the reaction interface respectively; (**c**) is the photograph of line scan in (**b**)).

Table 6. EDS analysis results for areas in Figure 11b.

Area No.	Elemental Compositions/(wt%)					Mineral Phases
	Fe	Al	Si	Ca	O	
1	69.12	1.02	0.00	0.00	29.86	Hematite
2	56.12	1.46	1.25	7.14	34.03	Dendritic SFCA
3	48.65	2.35	2.87	10.52	35.61	Lamellar SFCA
4	46.54	3.71	3.04	12.69	34.02	Disseminated SFCA
5	0.00	54.21	0.00	0.00	45.79	Residual alumina

Figure 12 and Table 10 indicate that diaspore with the average interfacial width of 1.72 mm possesses relatively better reactivity than free state alumina and gibbsite. In the reaction interface, the disseminated SCFA is gradually transformed into lamellar SFCA and then tabular or dendritic SFCA (Figure 12 and Table 7). Meanwhile, the corresponding iron content of SFCA is further increased, leading to higher strength of bonding phases. In addition, hematite as the major solid phase is more tightly bonded with SFCA. Furthermore, the porosity is lowered accordingly, attributed to the lower LOI of 15.76% than that of gibbsite. Therefore, diaspore is more favorable to the formation of higher quality bonding phases and tighter sinter microstructure compared with gibbsite and free state alumina.

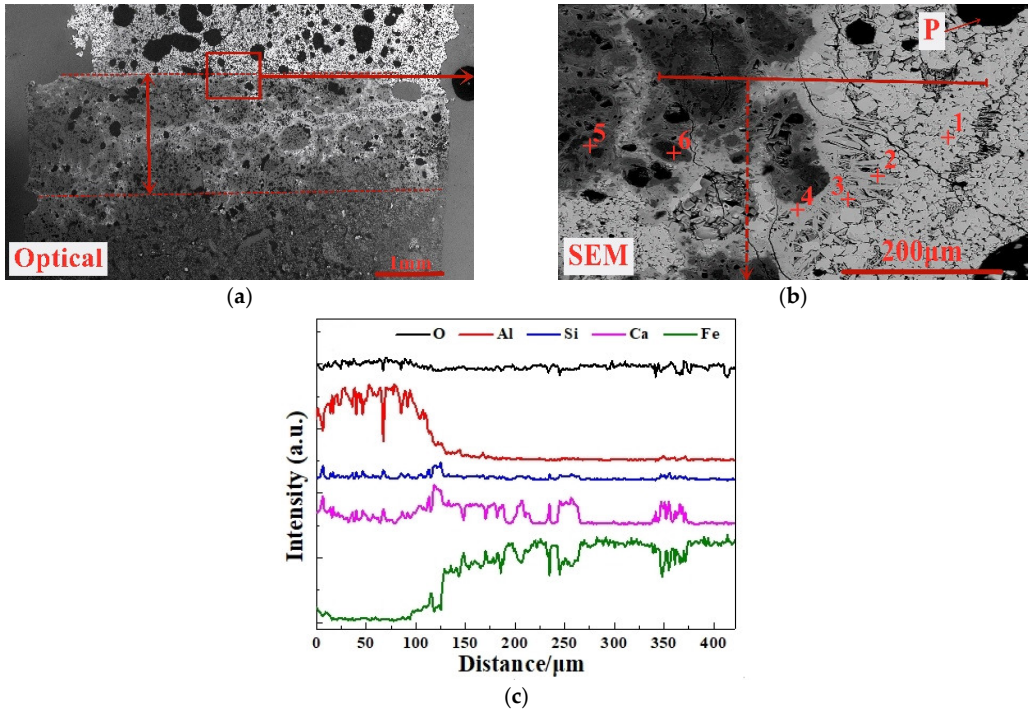

Figure 12. Effect of diaspore on the characteristics of the bonding matrix (P: Pore; a→b: Rotate 90° to the right; (**a**,**b**) are the optical and SEM photographs of the reaction interface respectively; (**c**) is the photograph of line scan in (**b**)).

Table 7. EDS analysis results for areas in Figure 12b.

Area No.	Elemental Compositions/(wt%)					Mineral Phases
	Fe	Al	Si	Ca	O	
1	69.34	0.37	0.00	0.00	30.29	Hematite
2	47.36	3.12	2.24	11.89	35.39	Tabular SFCA
3	56.68	1.22	1.28	6.78	34.04	Dendritic SFCA
4	48.87	2.32	2.56	10.31	35.94	Lamellar SFCA
5	46.83	3.45	2.78	12.11	34.83	Disseminated SFCA
6	0.00	54.38	0.00	0.00	45.62	Residual alumina

Figure 13 and Table 8 illustrate the mineralogy of reaction interface between the iron ore and kaolinite. The average interfacial width of 2.27 mm is greater than that of the above three types of alumina (Table 10), attributed to the excellent assimilability and relatively higher liquid phase fluidity. It can be observed that the extensive silicate phase is formed and evenly distributed on the side of the iron ore tablet due to the high SiO_2 content. Meanwhile, SFCA primarily occurs in tabular, dendritic, or acicular texture, indicating that kaolinite has a more favorable effect on the formation of higher strength SCFA than free state alumina, gibbsite, and diaspore. In addition, the major solid phase, i.e., hematite, is commendably wetted by the bonding phases and the porosity of reaction interface is reduced with the diffusion of liquid phases. Hence, kaolinite should be more beneficial for the sintering process compared with the above three types of alumina including free state alumina, gibbsite, and diaspore.

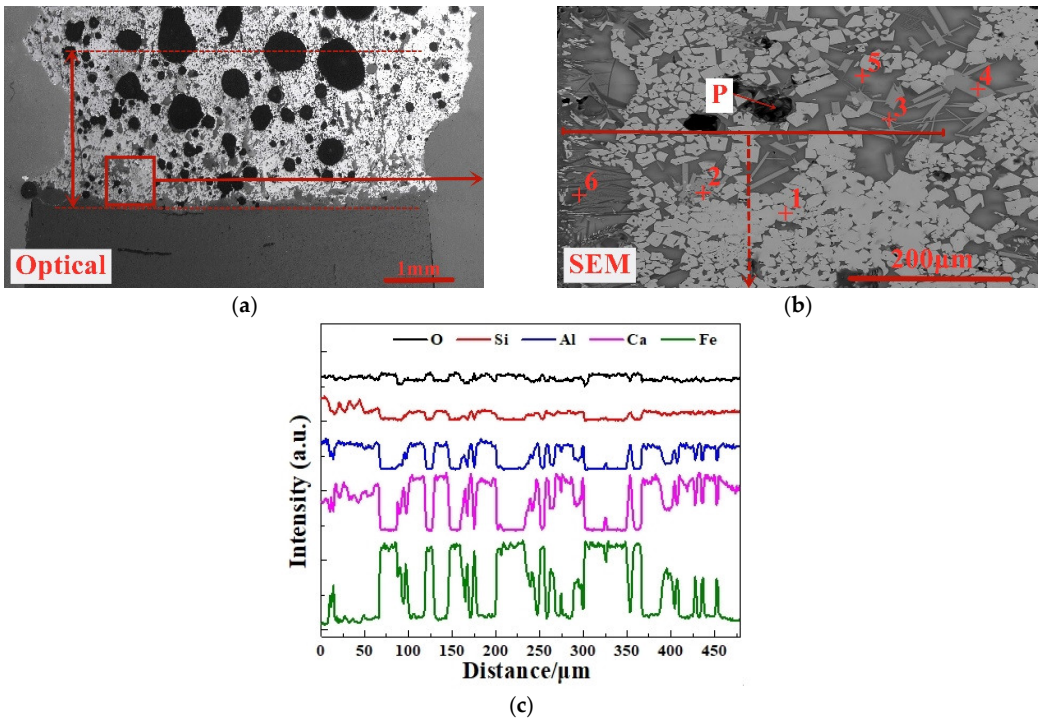

Figure 13. Effect of kaolinite on the characteristics of the bonding matrix (P: Pore; a→b: Rotate 90° to the right; (**a**,**b**) are the optical and SEM photographs of the reaction interface respectively; (**c**) is the photograph of line scan in (**b**)).

Table 8. EDS analysis results for areas in Figure 13b.

Area No.	Elemental Compositions/(wt%)					Mineral Phases
	Fe	Al	Si	Ca	O	
1	69.36	0.68	0.00	0.00	29.96	Hematite
2	57.85	0.78	1.10	5.67	34.60	Acicular SFCA
3	56.92	1.01	1.13	6.34	34.60	Dendritic SFCA
4	47.66	3.01	2.08	11.56	35.69	Tabular SFCA
5	28.39	5.23	22.79	27.45	16.14	Silicate
6	0.00	53.98	0.00	0.00	46.02	Residual alumina

As evidenced in Figure 14 and Table 10, the high reactivity of hercynite with the average interfacial width of 2.23 mm contributes to the further transformation from disseminated or lamellar SCFA further into dendritic or acicular SFCA. In addition, the formation amount of higher strength SFCA is increased significantly, owing to the migration of massive additional Fe^{3+} ions in hercynite into liquid phases (Figure 14 and Table 9). In addition, the much denser micro-texture of interweaving between hematite and SFCA is observed. In the meantime, a rather lower porosity of the reaction interface is obtained due to the excellent reactivity and lower LOI of hercynite. Thus, it is expected that alumina in the form of hercynite is more favorable to the iron ore sintering process compared with free state alumina, gibbsite, and diaspore. The relevant influence extent of hercynite should be close to that of kaolinite.

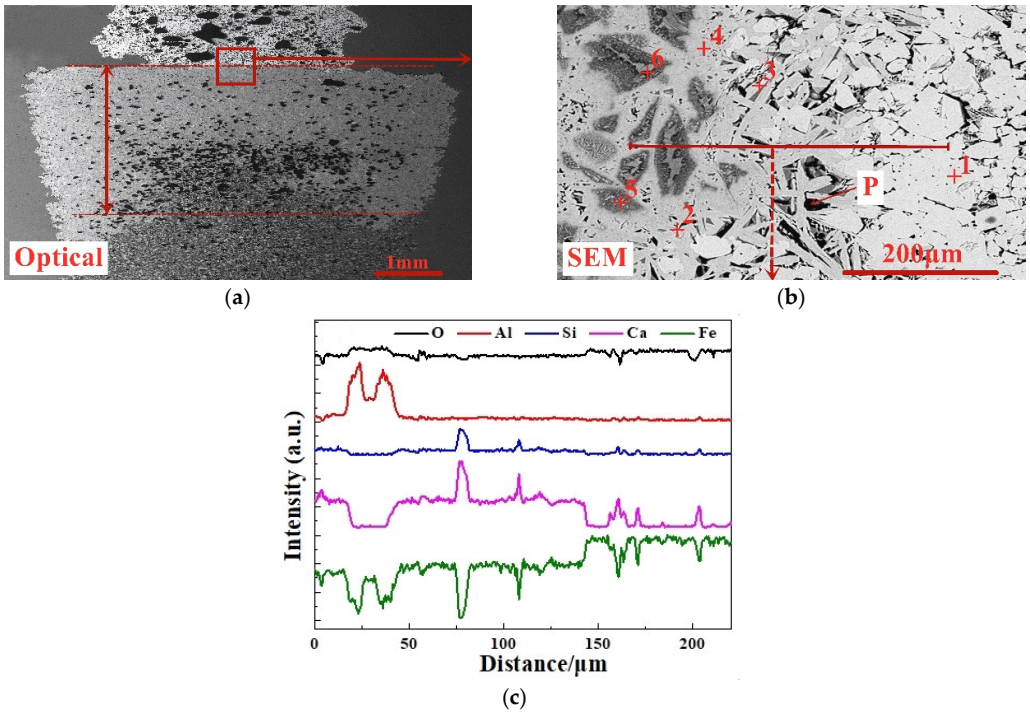

Figure 14. Effect of hercynite on the characteristics of the bonding matrix (P: Pore; a→b: Rotate 90° to the right; (**a**,**b**) are the optical and SEM photographs of the reaction interface respectively; (**c**) is the photograph of line scan in (**b**)).

Table 9. EDS analysis results for areas in Figure 14b.

Area No.	Elemental Compositions/(wt%)					Mineral Phases
	Fe	Al	Si	Ca	O	
1	69.72	0.74	0.00	0.00	29.54	Hematite
2	58.16	0.53	1.13	5.48	34.70	Acicular SFCA
3	57.02	1.12	1.21	6.28	34.37	Dendritic SFCA
4	48.94	2.12	2.37	9.89	36.68	Lamellar SFCA
5	47.11	3.18	2.59	11.77	35.35	Disseminated SFCA
6	0.00	54.21	0.00	0.00	45.79	Residual alumina

As investigated in the above, kaolinite possesses the highest reactivity and hercynite ranks the second, followed by diaspore and gibbsite, while the reactivity of free state alumina is the poorest (Table 10). The lower reactivity of alumina is, the more unreacted the alumina residue remains. The unreacted alumina is unable to commendably participate in liquid phase reaction and then greatly increases the viscosity of liquid phases. In order to achieve the more formation of liquid phases, more solid fuel consumption is needed during sintering. Consequently, the sintering temperature is supposed to be increased. As confirmed in the prior researches [29,36,48,49], higher sintering temperature contributes to the formation of lower strength SFCA such as tabular or disseminated SCFA. Thus, kaolinite and hercynite with better reactivity are more advantageous to the formation of higher strength SFCA such as dendritic or acicular SFCA, while free state alumina with rather poorer reactivity leads to the more formation of tabular or disseminated SCFA with lower strength. In the meantime, the denser micro-texture of interweaving between hematite and SFCA is formed in the reaction interface as alumina occurs in kaolinite or hercynite. Hence, it is considered that alumina in the form of kaolinite or hercynite would lead to higher sinter strength compared with other types of alumina. Gibbsite and diaspore could lead to a relatively lower sinter strength due to the deterioration of SFCA self-strength, while free state alumina is the most detrimental type of alumina for iron ore sintering. In the near future, the relevant sinter pot tests will be conducted to prove the influence of alumina concentration and type on the sintering performance of iron ores.

Table 10. The average interfacial width of different types of alumina (mm).

Alumina Types	Free State Alumina	Gibbsite	Diaspore	Kaolinite	Hercynite
Average interfacial width	1.31	1.61	1.72	2.27	2.23

4. Conclusions

On the basis of the investigations of alumina type of typical iron ores and its possible influence on high-temperature characteristics, the relevant different impacts of various alumina types and concentrations are revealed. Iron ores possess different high-temperature characteristics not only attributed to the difference of chemical compositions but also owing to their various alumina types. It is found that the assimilability of iron ores is weakened with the increase of Al_2O_3 content. However, the adverse influence extents of different types of alumina are quite different. Kaolinite leads to relatively better assimilability (<1330 °C), followed by hercynite, gibbsite, and diaspore, while free state alumina is extremely deleterious to assimilability. Moreover, the influence of alumina type on liquid phase fluidity of iron ores is comparatively complicated with the Al_2O_3 content varying. Higher Al_2O_3 content (≥1.5%) is confirmed harmful to the liquid phase fluidity, but the influence degrees are obviously different. Diaspore contributes to correspondingly higher liquid phase fluidity (>3), followed by kaolinite, free state alumina, hercynite, and gibbsite in turn. Remarkably, as the Al_2O_3 content is over 2.70%, the harmfulness of kaolinite on the liquid phase fluidity is increased dramatically to only next to that of gibbsite. Furthermore, kaolinite and hercynite have much more

positive effect on the formation of higher strength bonding phases such as dendritic or acicular SFCA due to the better reactivity. Extensive silicate is also observed in the reaction interface between the iron ore and kaolinite owing to the higher SiO_2 content of kaolinite. Gibbsite and diaspore are instrumental in forming relatively lower strength lamellar or tabular SFCA, while disseminated SCFA with a rather poorer strength is massively formed in the reaction interface with alumina in the form of free state alumina. Overall, kaolinite and hercynite are more beneficial for high-temperature characteristics of iron ores, followed by diaspore and gibbsite, while free state alumina possesses the most adverse impact. Combined with the impact of alumina concentration and type on high-temperature characteristics, the relevant influence on the sintering performance of iron ores will be elucidated in the future studies for better achieving the effective utilization of the abundant high-alumina iron ores.

Author Contributions: Conceptualization, D.Z., J.P., and L.L.; data curation, Y.X.; investigation, Y.X. and H.T.; methodology, Y.X., D.Z., and J.P.; resources, D.Z. and J.P.; supervision, Z.G. and C.Y.; writing—original draft, Y.X.; writing—review and editing, J.P. All authors have read and agreed to the published version of the manuscript.

Funding: This research was funded by the Youth Natural Science Foundation China, grant number (51904347), and the Major Project of Master Alloy Manufacture for Heat Resistant Stainless Steel Production, grant number (AA18242003).

Acknowledgments: Financial supports from the Youth Natural Science Foundation China, no. 51904347 and Major Project of Master Alloy Manufacture for Heat Resistant Stainless Steel Production, no. AA18242003 funded by the Provincial Government of Guangxi Zhuang Autonomous District, are sincerely acknowledged. We are also thankful to the Analytical and Testing Center of Central South University, which supplied us the facilities to fulfil the measurement.

Conflicts of Interest: The authors declare no conflict of interest.

Appendix A

Appendix A.1. Detailed Data of Size Distributions of Raw Materials

Tables A1 and A2 show the detailed data of size distributions of iron ores and Al-additives respectively, providing more information of raw materials.

Table A1. Detailed data of size distributions of iron ores.

Size/mm	0.15–0.5	0.074–0.15	0.045–0.074	−0.045
Iron ore A	6.10	41.80	43.15	8.95
Iron ore B	7.22	39.27	44.13	9.38
Iron ore C	7.89	43.36	42.52	6.23
Iron ore D	6.92	42.27	41.87	8.94
Iron ore E	8.06	44.19	38.59	9.16
Iron ore F	7.66	43.21	42.15	6.98
Iron ore G	8.39	42.78	40.36	8.47
Iron ore H	6.95	45.06	38.23	9.76

Table A2. Detailed data of size distributions of Al-additives.

Size/mm	0.074–0.15	0.045–0.074	−0.045
Al_2O_3 reagent	15.27	58.38	26.35
$Al(OH)_3$ reagent	16.62	59.89	23.49
Washed kaolinite	14.88	55.72	29.40
Synthetic hercynite	16.32	57.63	26.05
Diasporic bauxite	15.78	56.39	27.83

Appendix A.2. Mineralogy of Iron Ores

Figure A1 illustrates the main phases identified in the eight iron ores. Australian iron ores A, B and C mainly contain goethite, hematite and a small amount of quartz. Brazilian iron ores D and E and African iron ore F primarily consist of goethite, hematite and a certain content of quartz and gibbsite. The iron-bearing minerals of African iron ore G and Indian iron ore H are mainly hematite and trace goethite while the gangue minerals are different, which includes quartz, gibbsite and kaolinite in iron ore H and is only composed of quartz in iron ore G. It can be observed that the minerals in eight iron ores are different, which may lead to different types of alumina occurring in iron ores.

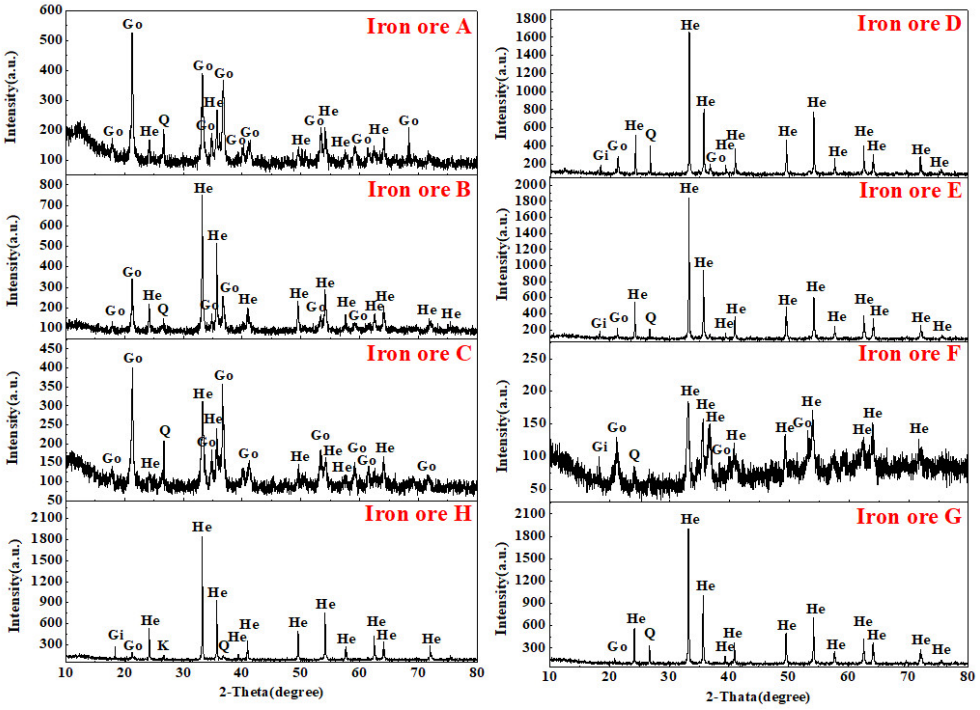

Figure A1. X-ray diffraction patterns of iron ores (Go-Goethite, He-Hematite, Q-Quartz, Gi-Gibbsite, K-Kaolinite).

Figure A2 describes the microstructure of iron ores. Combined with the results of Table A2 in the manuscript, alumina occurrence states of eight iron ores are different which is consistent with the description of Figure A1. In iron ore A, 89.80% alumina presents in goethite to form alumogoethite and 10.20% alumina resides in hematite, which are both in the form of hercynite through Al^{3+} ions substituted for Fe^{3+} ions [41]. Besides, goethite mainly exhibits earthy or vitreous and the former is rich in alumina as shown in Figure A2. Alumina of iron ores B and E mainly occurs in goethite, gibbsite and kaolinite while alumina in iron ores D and F is primarily concentrated in goethite and

gibbsite and in iron ores C and G is mostly found in goethite and kaolinite. Meanwhile, the occurrence states of alumina of iron ore H are relatively complex including hercynite, gibbsite and kaolinite with alumina mainly existing in hematite, goethite, gibbsite and kaolinite. The various occurrence states of alumina are supposed to have different effect on high-temperature characteristics of iron ores.

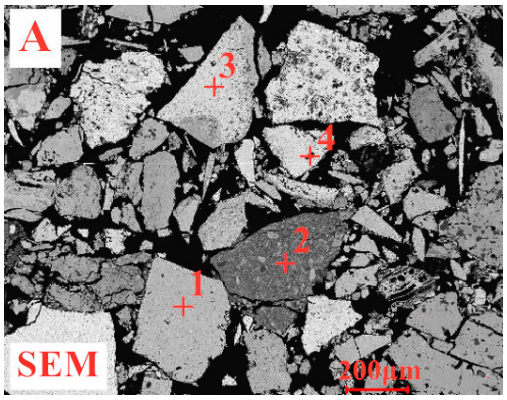

Area No.	Elemental compositions/(wt-%)					Mineral phases
	Fe	Al	Si	Ca	O	
1	59.39	1.27	0.32	0.12	38.90	Goethite
2	62.21	3.12	0.19	0.10	34.38	Goethite
3	65.42	4.35	0.27	0.11	29.85	Hematite
4	0.00	0.00	45.63	0.00	54.37	Quartz

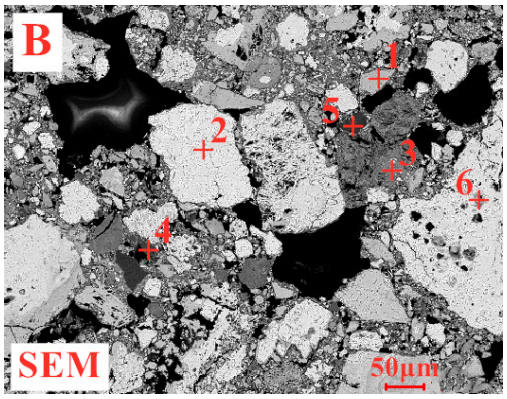

Area No.	Elemental compositions/(wt-%)					Mineral phases
	Fe	Al	Si	Ca	O	
1	60.12	1.02	0.24	0.06	38.56	Goethite
2	66.23	2.31	0.17	0.13	31.16	Hematite
3	62.36	2.78	0.26	0.11	34.49	Goethite
4	5.93	22.67	29.32	0.32	41.76	Kaolinite
5	9.56	39.25	0.54	0.28	50.37	Gibbsite
6	0.00	0.00	46.38	0.00	53.62	Quartz

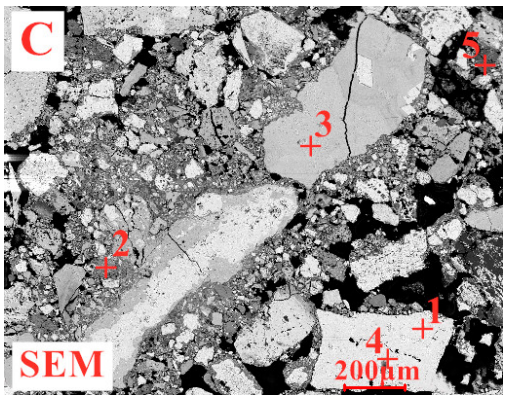

Area No.	Elemental compositions/(wt-%)					Mineral phases
	Fe	Al	Si	Ca	O	
1	65.89	2.14	0.22	0.09	31.66	Hematite
2	62.38	2.59	0.27	0.18	34.58	Goethite
3	59.86	1.12	0.26	0.15	38.61	Goethite
4	0.00	0.00	45.78	0.00	54.22	Quartz
5	4.38	25.32	30.16	0.29	39.85	Kaolinite

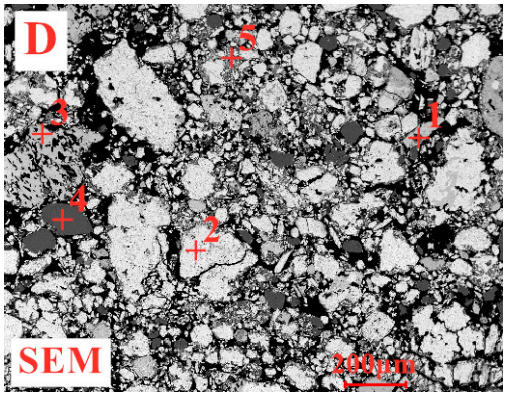

Area No.	Elemental compositions/(wt-%)					Mineral phases
	Fe	Al	Si	Ca	O	
1	0.00	0.00	46.72	0.00	53.28	Quartz
2	66.12	1.32	0.18	0.13	32.25	Hematite
3	62.11	2.94	0.33	0.12	34.50	Goethite
4	8.96	39.48	0.63	0.39	50.54	Gibbsite
5	59.93	3.82	0.43	0.26	35.56	Goethite

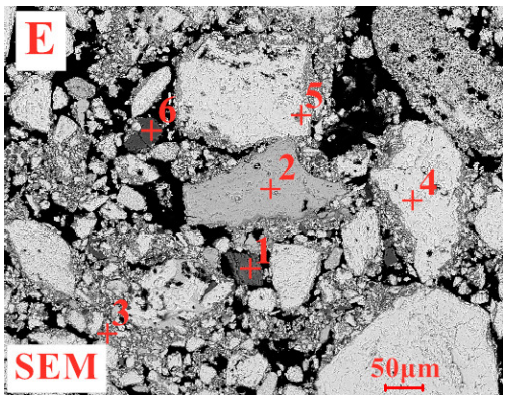

Area No.	Elemental compositions/(wt-%)					Mineral phases
	Fe	Al	Si	Ca	O	
1	8.32	20.13	26.72	0.39	44.44	Kaolinite
2	60.36	2.69	0.31	0.14	36.50	Goethite
3	63.54	1.13	0.18	0.05	35.10	Goethite
4	67.36	0.78	0.13	0.06	31.67	Hematite
5	0.00	0.00	45.87	0.00	54.13	Quartz
6	10.02	36.58	0.47	0.51	52.42	Gibbsite

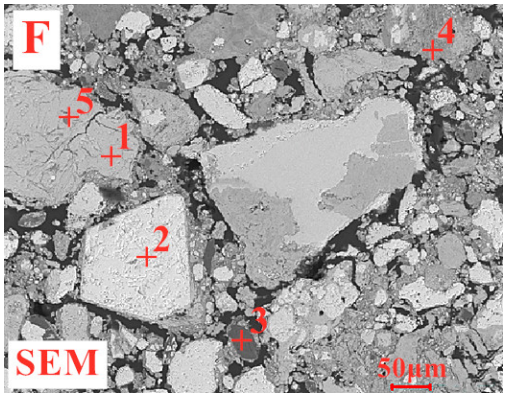

Area No.	Elemental compositions/(wt-%)					Mineral phases
	Fe	Al	Si	Ca	O	
1	59.67	3.97	0.23	0.10	36.03	Goethite
2	65.65	1.54	0.27	0.16	32.38	Hematite
3	8.46	41.23	0.87	0.34	49.10	Gibbsite
4	62.23	3.98	0.35	0.18	33.26	Goethite
5	0.00	0.00	45.33	0.00	54.67	Quartz

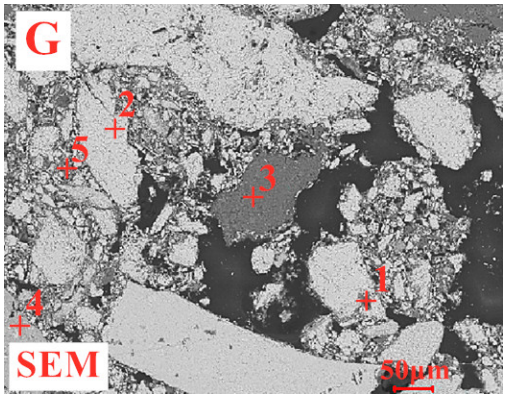

Area No.	Elemental compositions/(wt-%)					Mineral phases
	Fe	Al	Si	Ca	O	
1	0.00	0.00	46.38	0.00	53.62	Quartz
2	66.91	1.01	0.12	0.07	31.89	Hematite
3	9.59	21.27	27.35	0.14	41.65	Kaolinite
4	62.88	3.28	0.29	0.17	33.38	Goethite
5	60.52	1.76	0.38	0.08	37.26	Goethite

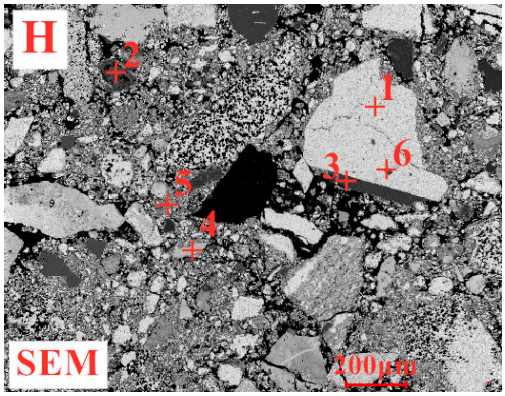

Area No.	Elemental compositions/(wt-%)					Mineral phases
	Fe	Al	Si	Ca	O	
1	66.36	1.24	0.21	0.07	32.12	Hematite
2	6.12	21.38	28.69	0.31	43.50	Kaolinite
3	9.68	38.49	0.59	0.35	50.89	Gibbsite
4	60.39	1.11	0.28	0.12	38.10	Goethite
5	62.48	2.53	0.24	0.09	34.66	Goethite
6	0.00	0.00	46.22	0.00	53.78	Quartz

Figure A2. (**A–D**)The microstructure of Australian and Indian iron ores, (**E–H**) The microstructure of Brazilian and African iron ores.

Appendix A.3. Starting Material Compositions

The experimental run table with a clear inventory of the starting material compositions for all the experiments is shown in Tables A3 and A4.

Table A3. Starting material compositions for the experiments of assimilability (wt%).

Alumina Type	Alumina Concentration	TFe	SiO_2	CaO	Al_2O_3	MgO
Free state alumina	1.50	64.24	5.00	0.06	1.50	0.11
	2.00	63.90	5.00	0.06	2.00	0.11
	2.50	63.55	5.00	0.06	2.50	0.11
	3.00	63.20	5.00	0.06	3.00	0.11
	3.50	62.86	5.00	0.06	3.50	0.11
Gibbsite	1.50	64.23	5.00	0.06	1.50	0.11
	2.00	63.88	5.00	0.06	2.00	0.11
	2.50	63.52	5.00	0.06	2.50	0.11
	3.00	63.17	5.00	0.06	3.00	0.11
	3.50	62.82	5.00	0.06	3.50	0.11
Diaspore	1.50	64.23	5.00	0.07	1.50	0.11
	2.00	63.87	5.00	0.07	2.00	0.11
	2.50	63.51	5.00	0.07	2.50	0.11
	3.00	63.15	5.00	0.07	3.00	0.11
	3.50	62.78	5.00	0.08	3.50	0.11
Kaolinite	1.50	64.23	5.00	0.06	1.50	0.11
	2.00	63.87	5.00	0.06	2.00	0.11
	2.50	63.50	5.00	0.06	2.50	0.11
	3.00	63.14	5.00	0.06	3.00	0.11
	3.50	62.71	5.00	0.06	3.50	0.11
Hercynite	1.50	64.22	5.00	0.06	1.50	0.12
	2.00	63.85	5.00	0.06	2.00	0.13
	2.50	63.47	5.00	0.07	2.50	0.14
	3.00	63.10	5.00	0.07	3.00	0.15
	3.50	62.72	5.00	0.07	3.50	0.16

Table A4. Starting material compositions for the experiments of liquid phase fluidity (wt%).

Alumina Type	Alumina Concentration	TFe	SiO_2	CaO	Al_2O_3	MgO
Free state alumina	1.50	50.55	5.00	19.97	1.50	0.09
	2.00	50.21	5.00	19.97	2.00	0.08
	2.50	49.87	5.00	19.97	2.50	0.08
	3.00	49.53	5.00	19.97	3.00	0.08
	3.50	49.19	5.00	19.97	3.50	0.08
Gibbsite	1.50	50.53	5.00	19.99	1.50	0.08
	2.00	50.18	5.00	19.99	2.00	0.08
	2.50	49.83	5.00	19.98	2.50	0.08
	3.00	49.45	5.00	20.01	3.00	0.08
	3.50	49.09	5.00	20.01	3.50	0.08
Diaspore	1.50	50.54	5.00	19.97	1.50	0.08
	2.00	50.16	5.00	19.99	2.00	0.08
	2.50	49.79	5.00	20.01	2.50	0.08
	3.00	49.41	5.00	20.03	3.00	0.08
	3.50	49.09	5.00	19.99	3.50	0.08
Kaolinite	1.50	50.50	5.00	20.02	1.50	0.09
	2.00	50.14	5.00	20.02	2.00	0.09
	2.50	49.77	5.00	20.03	2.50	0.09
	3.00	49.42	4.99	20.03	3.00	0.08
	3.50	49.04	5.00	20.04	3.50	0.08
Hercynite	1.50	50.47	5.00	20.02	1.50	0.10
	2.00	50.11	5.00	20.01	2.00	0.11
	2.50	49.73	5.00	20.02	2.50	0.12
	3.00	49.37	5.00	20.01	3.00	0.13
	3.50	49.01	5.00	20.00	3.50	0.14

Appendix A.4. Correlation between Chemical Compositions (SiO_2 and Al_2O_3) and Liquid Phase Fluidity of Iron Ores

As shown in Figure A3, the amount of (SiO_2 + SiO_2/Al_2O_3) possesses fairly better linear positive correlation with liquid phase fluidity and the linear correlation coefficient reaches as high as 0.94251. Here, (SiO_2 + SiO_2/Al_2O_3) is mainly regarded as a parameter to expound the collective influence of SiO_2 and Al_2O_3 on liquid phase fluidity. It is inadequate to only take into consideration of the influence of SiO_2 or Al_2O_3. This also provides guidance for the sequential studies of the influence of alumina concentration and type on high-temperature characteristics. Namely, SiO_2 content of sinter sinter mixture should be remained at the same level in the follow-up experiments.

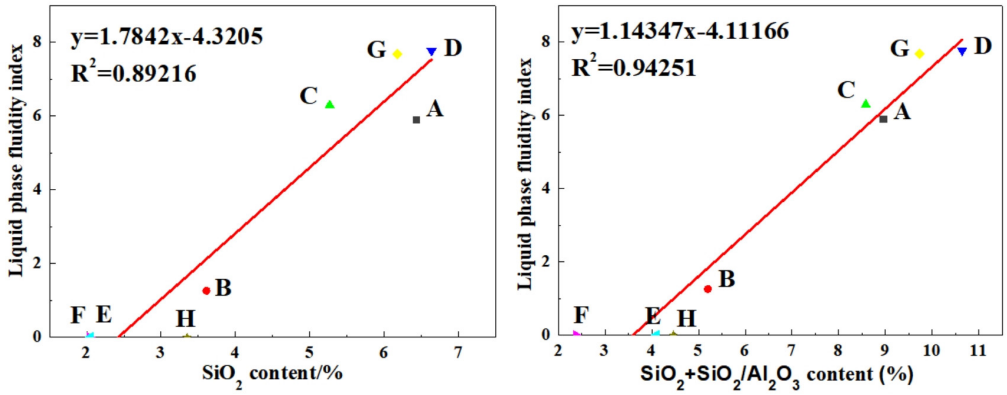

Figure A3. Correlation between chemical compositions and liquid phase fluidity of iron ores.

References

1. Umadevi, T.; Deodar, A.V.; Mahapatra, P.C.; Prabhu, M.; Ranjan, M. Influence of alumina on iron ore sinter properties and productivity in the conventional and selective granulation sintering process. *Steel Res. Int.* **2009**, *80*, 686–692.
2. Fernandez-Gonzalez, D.; Ruiz-Bustinza, I.; Mochon, J.; Gonzalez-Gasca, C.; Verdeja, L.F. Iron ore sintering: raw materials and granulation. *Min. Process. Extr. Metall. Rev.* **2017**, *38*, 36–46.
3. Fernandez-Gonzalez, D.; Ruiz-Bustinza, I.; Mochon, J.; Gonzalez-Gasca, C.; Verdeja, L.F. Iron ore sintering: quality indices. *Min. Process. Extr. Metall. Rev.* **2017**, *38*, 254–264.
4. Hino, M.; Nagasaka, T.; Katsumata, A.; Higuchi, K.-I.; Yamaguchi, K.; Kon-No, N. Simulation of primary-slag melting behavior in the cohesive zone of a blast furnace, considering the effect of Al_2O_3, Fe_tO, and basicity in the sinter ore. *Metall. Mater. Trans.* **1999**, *30*, 671–683.
5. Wu, S.; Huang, W.; Kou, M.; Liu, X.; Du, K.; Zhang, K. Influence of Al_2O_3 Content on Liquid Phase Proportion and Fluidity of Primary Slag and Final Slag in Blast Furnace. *Steel Res. Int.* **2015**, *86*, 550–556.
6. Das, S.K.; Das, B.; Sakthivel, R.; Mishra, B.K. Mineralogy, microstructure, and chemical composition of goethites in some iron ore deposits of orissa, India. *Min. Process. Extr. Metall. Rev.* **2010**, *31*, 97–110.
7. Liu, D.; Loo, C.E.; Evans, G. Flow characteristics of the molten mix generated during iron ore sintering. *Int. J. Miner. Process.* **2016**, *149*, 56–68.
8. Lu, L.; Holmes, R.J.; Manuel, J.R. Effects of Alumina on Sintering Performance of Hematite Iron Ores. *ISIJ Int.* **2007**, *47*, 349–358.
9. Zhang, G.-L.; Wu, S.; Su, B.; Que, Z.-G.; Hou, C.-G.; Jiang, Y. Influencing factor of sinter body strength and its effects on iron ore sintering indexes. *Int. J. Miner. Metall. Mater.* **2015**, *22*, 553–561.
10. Chai, Y.F.; Wu, W.T.; Zhang, J.L.; An, S.L.; Peng, J.; Wang, Y.Z. Influencing mechanism of Al_2O_3 on sintered liquid phase of iron ore fines based on thermal and kinetic analysis. *Ironmak. Steelmak.* **2019**, *46*, 424–430.
11. Hapugoda, S.; Lu, L.; Donskoi, E.; Manuel, J. Mineralogical quantification of iron ore sinter. *Min. Process. Extr. Metall. Trans.* **2016**, *125*, 156–164.
12. Lu, L.; Ishiyama, O. Recent advances in iron ore sintering. *Min. Process. Extr. Metall. Trans.* **2016**, *125*, 132–139.
13. Wu, S.; Zhang, G. Liquid Absorbability of Iron Ores and Large Limonite Particle Divided Adding Technology in the Sintering Process. *Steel Res. Int.* **2015**, *86*, 1014–1021.
14. Yan, B.-J.; Zhang, J.-L.; Guo, H.-W.; Chen, L.-K.; Li, W. High-temperature performance prediction of iron ore fines and the ore-blending programming problem in sintering. *Int. J. Miner. Metall. Mater.* **2014**, *21*, 741–747.
15. Yu, Z.W.; Qian, L.X.; Long, H.M.; Wang, Y.F.; Meng, Q.M.; Chun, T.J. Determination method of high-temperature characteristics of iron-ore sintering based on $n(Fe_2O_3)/n(CaO)$. *J. Iron. Steel Res. Int.* **2019**, *26*, 1257–1264.
16. Pei, Y.-D.; Wu, S.; Shao, X.-J.; Zhao, Z.-X.; An, G.; Ma, Z.-J.; Zhang, W.-D. Establishment and industrial practice of high-temperature process evaluation system in sintering. *J. Iron Steel Res. Int.* **2018**, *25*, 910–922.
17. Ware, N.; Manuel, J. Fundamental nucleus assimilation behaviour of haematite and goethite containing ores in iron ore sintering. *Min. Process. Extr. Metall.* **2016**, *125*, 149–155.

18. Qian, L.-X.; Zhang, Y.-D.; Long, H.-M.; Meng, Q.-M.; Li, N. Effect of gangue composition on assimilation characteristic of iron ore in the sintering process. *Ironmak. Steelmak.* **2019**, *16*, 1–7.
19. Wu, S.; Zhang, G.; Chen, S.; Su, B. Influencing Factors and Effects of Assimilation Characteristic of Iron Ores in Sintering Process. *ISIJ Int.* **2014**, *54*, 582–588.
20. Wu, S.; Zhai, X.-B. Factors influencing melt fluidity of iron ore. *Metall. Res. Technol.* **2018**, *115*, 505.
21. Kasai, E.; Sakano, Y.; Nakamura, T. Influence of iron ore properties on the flow of melt formed in the sintering process. *Tetsu-to-Hagane* **2000**, *86*, 139–145.
22. Maeda1, T.; Nishioka, K.; Nakashima, K.; Shimizu, M. Formation rate of calcium ferrite melt focusing on SiO_2 and Al_2O_3 component. *ISIJ Int.* **2004**, *44*, 2046–2051.
23. Sinha, M.; Nistala, S.H.; Chandra, S.; Mankhand, T.R. Thermodynamic study of evolution of sinter phases at different alumina level. *Ironmak. Steelmak.* **2017**, *44*, 1–8.
24. Guo, H.; Guo, X. Effect of alumina on liquid phase formation in sintering process of iron ore fines. *Steel Res. Int.* **2019**, *90*, 1900138.
25. Ooi, T.C.; Campbell-Hardwick, S.; Zhu, D.; Pan, J. Sintering Performance of Magnetite-Hematite-Goethite and Hematite-Goethite Iron Ore Blends and Microstructure of Products of Sintering. *Miner. Process. Extr. Metall. Rev.* **2013**, *35*, 266–281.
26. Ono, H.; Dohi, Y.; Arikata, Y.; Usui, T. Effect of mineral composition and pore structure on reducibility of composite iron ore sinter. *ISIJ Int.* **2009**, *49*, 722–728.
27. Wu, S.; Li, H.; Zhang, W.; Su, B. Effect of thermodynamic melt formation characteristics on liquid phase fluidity of iron ore in the sintering process. *Metals* **2019**, *9*, 404.
28. Chen, C.; Lu, L.; Jiao, K. Thermodynamic modelling of iron ore sintering reactions. *Miner.* **2019**, *9*, 361.
29. Scarlett, N.V.Y.; Pownceby, M.I.; Madsen, I.C.; Christensen, A.N. Reaction sequences in the formation of silico-ferrites of calcium and aluminum in iron ore sinter. *Metall. Mater. Trans. B* **2004**, *35*, 929–936.
30. Ji, Z.; Zhao, Y.; Gan, M.; Fan, X.; Chen, X.; Hu, L. Microstructure and Minerals Evolution of Iron Ore Sinter: Influence of SiO_2 and Al_2O_3. *Minerals* **2019**, *9*, 449.
31. Patrick, T.R.; Pownceby, M.I. Stability of silico-ferrite of calcium and aluminum (SFCA) in air-solid solution limits between 1240 °C and 1390 °C and phase relationships within the Fe_2O_3-CaO-Al_2O_3-SiO_2 (FCAS) system. *Metall. Mater. Trans. B* **2002**, *33*, 79–89.
32. Kalenga, M.K.; Garbers-Craig, A.M. Investigation into how the magnesia, silica, and alumina contents of iron ore sinter influence its mineralogy and properties. *J. South. Afr. Inst. Min. Metall.* **2010**, *110*, 447–456.
33. Park, T.J.; Choi, J.S.; Min, D.J. Investigation of the effects of Al_2O_3 content and cooling rate on crystallization in Fe_2O_3–CaO–Al_2O_3 system using in situ confocal laser scanning microscopy. *Steel Res. Int.* **2019**, *90*, 1900001.
34. Dong, J.-J.; Wang, G.; Gong, Y.G.; Xue, Q.G.; Wang, J.S. Effect of high alumina iron ore of gibbsite type on sintering performance. *Ironmak. Steelmak.* **2015**, *42*, 34–40.
35. O'Dea, D.P.; Ellis, B.G. New insights into alumina types in iron ore and their effect on sintering. In Proceedings of the 10th CSM Steel Congress, Shanghai, China, 21–23 October 2015.
36. Pownceby, M.I.; Webster, N.A.S.; Manuel, J.R.; Ware, N. The influence of ore composition on sinter phase mineralogy and strength. *Miner. Process. Extr. Met.* **2016**, *125*, 140–148.
37. Zhang, G.-L.; Wu, S.; Chen, S.-G.; Su, B.; Que, Z.; Hou, C.-G. Influence of gangue existing states in iron ores on the formation and flow of liquid phase during sintering. *Int. J. Miner. Metall. Mater.* **2014**, *21*, 962–968.
38. Webster, N.A.S.; O'Dea, D.P.; Ellis, B.G.; Pownceby, M.I. Effects of Gibbsite, Kaolinite and Al-rich Goethite as Alumina Sources on Silico-Ferrite of Calcium and Aluminium (SFCA) and SFCA-I Iron Ore Sinter Bonding Phase Formation. *ISIJ Int.* **2017**, *57*, 41–47.
39. Liao, F.; Guo, X.-M. The Effects of Al_2O_3 and SiO_2 on the formation process of Silico-Ferrite of Calcium and Aluminum (SFCA) by solid-state reactions. *Miner.* **2019**, *9*, 101.
40. Lv, X.; Bai, C.; Deng, Q.; Huang, X.; Qiu, G. Behavior of liquid phase formation during iron ores sintering. *ISIJ Int.* **2011**, *51*, 722–727.
41. Jiang, P.; Chen, J.-H.; Yan, M.-W.; Li, B.; Su, J.-D.; Hou, X. Morphology characterization of periclase–hercynite refractories by reaction sintering. *Int. J. Miner. Metall. Mater.* **2015**, *22*, 1219–1224.
42. Zhou, M.; Jiang, T.; Yang, S.-T.; Xue, X. Vanadium–titanium magnetite ore blend optimization for sinter strength based on iron ore basic sintering characteristics. *Int. J. Miner. Process.* **2015**, *142*, 125–133.

43. Matsumura, M.; Hoshi, M.; Kawaguchi, T. Improvement of sinter softening property and reducibility by controlling chemical compositions. *ISIJ Int.* **2005**, *45*, 594–602.
44. Li, H.; Wu, S.; Hong, Z.; Zhang, W.; Zhou, H.; Kou, M. The Mechanism of the effect of Al_2O_3 content on the liquid phase fluidity of iron ore fines. *Processes* **2019**, *7*, 931.
45. Wang, Z.; Pinson, D.; Chew, S.; Monaghan, B.J.; Pownceby, M.I.; Webster, N.A.S.; Rogers, H.; Zhang, G. Effects of sintering materials and gas conditions on formation of silico-ferrites of calcium and aluminium during iron ore sintering. *ISIJ Int.* **2016**, *56*, 1138–1147.
46. Machida, S.; Nushiro, K.; Ichikawa, K.; Noda, H.; Sakai, H. Experimental evaluation of chemical composition and viscosity of melts during iron ore sintering. *ISIJ Int.* **2005**, *45*, 513–521.
47. De Magalhães, M.S.; Brandão, P.R.G. Microstructures of industrial sinters from Quadrilatero Ferrifero's iron ores, Minas Gerais state, Brazil. *Miner. Eng.* **2003**, *16*, 1251–1256.
48. Webster, N.A.S.; Pownceby, M.I.; Madsen, I.C.; Studer, A.J.; Manuel, J.R.; Kimpton, J.A. Fundamentals of Silico-Ferrite of Calcium and Aluminum (SFCA) and SFCA-I iron ore sinter bonding phase formation: effects of $CaO:SiO_2$ ratio. *Metall. Mater. Trans. B* **2014**, *45*, 2097–2105.
49. Guo, H.; Guo, X.-M. Effect of aluminum dissolved in hematite on formation of Calcium Ferrites at 1473 K. *Metall. Mater. Trans. B* **2018**, *49*, 1974–1984.